Hydrodynamic Modelling of Flow Impact on Structures under Extreme Flow Conditions

LIANG Qiuhua[1,2*], CHEN Kaicui[1], HOU Jingming[2], XIONG Yan[1], WANG Gang[1], QIANG Juan[1]
[1] Key Laboratory of Coastal Disaster and Defence (Hohai University), Ministry of Education, Nanjing 210098, China
[2]School of Civil Engineering and Geosciences, Newcastle University
Newcastle upon Tyne, England, UK
[*]E-mail: Qiuhua.Liang@ncl.ac.uk

ABSTRACT
Apart from direct threat to human lives, flood events as a result of rapid catchment response to intense rainfall, failure of flood defences, tsunami or storm surge may induce huge impact forces on structures, causing structural damage or even failure. Most of the existing design codes do not properly account for these impact forces due to limited understanding of the underlying physical processes and lack of reliable empirical formulae or numerical approaches to quantifying them. This work aims to carry out laboratory experiments to better understand the interaction between the extreme flow hydrodynamics and hydraulic structures and use the measured data to validate a numerical model. The model solves the two-dimensional shallow water equations using a finite volume Godunov-type scheme for reliable simulation of complex flow hydrodynamics. New model component is included for estimating hydrostatic and hydrodynamic pressure to quantify flow impact on structures. The model is applied to reproduce two selected experiment tests with different settings and satisfactory numerical results are obtained, which confirms its predictive capability. The model will therefore provide a potential tool for wider and more flexible field-scale applications.

KEY WORDS: Wave-structure interaction; extreme flow conditions; flood hazards; shallow flow model; laboratory experiments.

1. Introduction

Flood events as a result of rapid catchment response to intense rainfall, failure of flood defences, tsunami or storm surge are usually highly transient in nature and featured with extreme flow conditions. Apart from their direct threat to human lives, the resulting rapidly varying flood waves may also create tremendous impact forces on structures, causing structural damage or even failure. For instance, the 2011 east Japan tsunami killed more than 15000 people and significantly damaged or destroyed numerous buildings, bridges and other infrastructure, in what can be described as one of the most advanced economies and most earthquake-prepared nations on earth. A large number of papers and reports have been published to document the field surveys to show the significant structure damage caused by this and other tsunami events [1-3]. In 2005, Hurricane Katrina together with the subsequent floods caused at least 1,833 people died and $108 billion (2005 USD) property damage. Then in 2012, Superstorm Sandy, the largest Atlantic hurricane on record, affected 24 states in USA and several other countries, killed 286 people along its path and left over $68 billion (2013 USD) in damage. In the UK, a flash flood following an intense rainfall event caused substantial damage to the historic Cornish town of Boscastle in 2004, with some 70 properties flooded, and over 100 cars, caravans, and several boats washed into the sea. There are numerous similar events worldwide that can be also listed here. Supported by a number of recent studies, it is generally recognised that meteorological and hydrological extremes, including storms and different types of floods, will become more frequent and cause more significant economic losses throughout the 21st century [4-6]. Therefore, it is necessary to review the current building practice and update our design and construction approaches in order to build more resilient communities under climate change.

In urban areas, some research has been carried out into the different types of loading induced on buildings due to floods [7-9]. Kelman and Spence [7] gave a good overview of the various potential forces that arise during a flood event, and pointed out that the actions most important to flood damage assessment are the lateral pressure imparted by the different height of water inside and outside of the building and the lateral pressure due to water velocity. However, less research has been reported to quantify these flood impacts. Therefore the current practical

[*] **Biography**: LIANG Qiuhua (1974-), Male, Ph. D., Professor.

design still commonly relies on the use of empirical formulas to obtain rough and unverified estimation of these hydraulic loadings to inform design.

On coastal flooding, assessments have been carried out into the modes of structural failure due to storm surge or tsunami, e.g. in New Orleans after Hurricane Katrina in 2005 [10-11]. However, as pointed out by Nistor et al. [3], most of the existing design codes do not properly take into accounts the impact forces from extreme hydraulic conditions caused by tsunamis and other analogous events. Similar to the urban applications, the existing empirical formulas for quantifying these forces for design present significant disagreement with observations. Therefore, there is an urgent need for new research effort to address the current knowledge gap. The new knowledge and tools are crucial for evaluating more reliably the possible structure damage caused by extreme flow conditions induced by tsunamis or other extreme disastrous events, which will in turn provide better guidelines and codes for city planning and structural design.

In the last two decades, numerous two-dimensional hydrodynamic modelling tools have been developed and widely applied to simulate different types of floods [12-21]. Most of these applications focus on estimating flood extent and water depth, which are then used to assess flood damages without considering the actual hydraulic impacts on the structures. These models, particularly the shock-capturing hydrodynamic flood models, can actually predict detailed velocity field and flow depth during a simulation, which may be extended to directly evaluate hydraulic loads on structures caused by different types of floods. Ghadimi and Reisinezhad [22] reports an attempt to assess flood impact on the cylindrical piers using a finite element shallow water model integrated with a formula derived from the Bernoulli principle for calculating pressure forces.

Reflecting the current research need, this work aims to present laboratory experiments to better understand the interaction between the extreme flow hydrodynamics and structures and provide the experimental measurements to validate a two-dimensional depth-averaged shallow flow model. The model solves the two-dimensional shallow water equations using a finite volume Godunov-type scheme, enabling automatic tracking of wet-dry fronts [23]. A new component is developed to calculate hydrostatic and hydrodynamic pressures and the corresponding forces. The model is suitable for evaluate flood impacts for different types of floods including those extreme events driven by tsunamis, storm surges and flash floods. The formulas for pressure calculation are different from those used by Ghadimi and Reisinezhad[22] and validated by new experimental measurements. The model may provide a robust tool for more flexible field-scale applications.

2. Numerical Model

2.1 Governing equations

The shallow water equations (SWEs) have been used to describe a wide range of flow hydrodynamics with horizontal dimensions much larger than water depth, including the discontinuous dam-break waves. Therefore, the hyperbolic conservation laws of SWEs are adopted in this work as the mathematical model for quantifying fluid-structure interaction under extreme flow conditions. In a matrix form, the governing equations may be written as

$$\frac{\partial \mathbf{q}}{\partial t}+\frac{\partial \mathbf{f}}{\partial x}+\frac{\partial \mathbf{g}}{\partial y}=\mathbf{s} \tag{1}$$

where t, x and y respectively represent the time and the two horizontal coordinates, $\mathbf{q}$, $\mathbf{f}$, $\mathbf{g}$ and $\mathbf{s}$ are the vectors of flow variables, x- and y-direction fluxes and the source terms, which are provided as follows when neglecting the Coriolis effects and the surface stresses

$$\mathbf{q}=\begin{bmatrix}\eta & uh & vh\end{bmatrix}^{\mathrm{T}};\quad \mathbf{f}=\begin{bmatrix}uh & u^2h+g(\eta^2-2\eta z_b)/2 & uvh\end{bmatrix}^{\mathrm{T}};\quad \mathbf{g}=\begin{bmatrix}vh & uvh & v^2h+g(\eta^2-2\eta z_b)/2\end{bmatrix}^{\mathrm{T}};$$

$$\mathbf{s}=\begin{bmatrix}0 & -C_f u\sqrt{u^2+v^2}-g\eta\,\partial z_b/\partial x & -C_f v\sqrt{u^2+v^2}-g\eta\,\partial z_b/\partial y\end{bmatrix}^{\mathrm{T}} \tag{2}$$

where η is the water level above datum, u and v are the x- and y-direction depth-averaged velocity components, $h = \eta - z_b$ is the total water depth with z_b being the bed elevation above datum, g represents the acceleration due to gravity, $C_f = gn^2/h^{1/3}$ calculates the bed roughness coefficient with n being the Manning coefficient, $-\partial z_b/\partial x$ and $-\partial z_b/\partial y$ are the bed slopes in the x- and y-direction. These vector terms were derived in Liang and Borthwick [24] by adopting the water level, instead of water depth, as one of the flow variables, which automatically ensure the well-balanced solution [25] of the lake at rest problem.

2.2 Numerical method

The numerical model employed in this work solves the above SWEs using a second-order finite volume Godunov-type scheme implemented with an HLLC approximate Riemann solver [26] for evaluating interface fluxes. The

second-order accuracy in both space and time is achieved by implementing the two-step MUSCL-Hancock method through a predictor step and a corrector step. The predictor step predicts intermediate values of the flow variables over a half time step $\Delta t/2$ using the following formula

$$\mathbf{q}_{i,j}^{k+1/2} = \mathbf{q}_{i,j}^{k} - \frac{\Delta t}{2\Delta x}\left(\mathbf{f}(\mathbf{q}_E^-) - \mathbf{f}(\mathbf{q}_W^+)\right) - \frac{\Delta t}{2\Delta y}\left(\mathbf{g}(\mathbf{q}_N^-) - \mathbf{g}(\mathbf{q}_S^+)\right) + \frac{\Delta t}{2}\mathbf{s}_{i,j}^{k} \tag{3}$$

where *i* and *j* are the cell indices, *E*, *W*, *N* and *S* denote the 'East', 'West', 'North' and 'South' cell interfaces, *k* represents the time level, and '–' and '+' indicate the left and right hand sides of an arbitrary cell interface, Δx and Δy are the cell sizes in the two Cartesian directions. In order to evaluate the flux functions $\mathbf{q}_E^-$, $\mathbf{q}_W^+$, $\mathbf{q}_N^-$ and $\mathbf{q}_S^+$, the face values of the flow variables must be firstly reconstructed at the mid-points of all four cell interfaces using the MUSCL linear reconstruction [27]. Taking the eastern interface as an example, $\mathbf{q}_E^-$ can be reconstructed by

$$\mathbf{q}_E^- = \mathbf{q}_{i,j}^{k} + \frac{\Delta x}{2}\nabla\hat{\mathbf{q}}_{i,j} \tag{4}$$

where $\nabla\hat{\mathbf{q}}_{i,j}$ is the gradient of flow variables restricted by a TVD Minmod slope limiter [24]. $\mathbf{q}_W^+$, $\mathbf{q}_N^-$ and $\mathbf{q}_S^+$ may be obtained through a similar reconstruction procedure. These face values of flow variables are then used to calculate the fluxes. To update flow variables over $\Delta t/2$ using (3), the source terms must also be properly discretized and can be simply achieved using a central-differencing scheme due to the use of the pre-balanced governing equations (1) and (2). It should be noted that, after reconstructing the face values of flow variables and bed level, the calculation for the predictor step is achieved entirely within cell (*i*, *j*) and no Riemann solution is involved.

The corrector step of the MUSCL-Hancock method updates the flow variables over a full time step using the following time-marching formula

$$\mathbf{q}_{i,j}^{k+1} = \mathbf{q}_{i,j}^{k} - \frac{\Delta t}{\Delta x}\left(\mathbf{f}_E - \mathbf{f}_W\right) - \frac{\Delta t}{\Delta y}\left(\mathbf{g}_N - \mathbf{g}_S\right) + \Delta t\mathbf{s}_{i,j}^{k+1/2} \tag{5}$$

where $\mathbf{f}_E$, $\mathbf{f}_W$, $\mathbf{g}_N$ and $\mathbf{g}_S$ are the four Godunov-type numerical fluxes obtained by solving the local Riemann problems defined respectively at each of the four interfaces of cell under consideration, e.g.

$$\mathbf{f}_E = F(\mathbf{q}_E^-, \mathbf{q}_E^+) \tag{6}$$

where $\mathbf{q}_E^-$ and $\mathbf{q}_E^+$ are the so-called Riemann states and are essentially the reconstructed values of the flow variables at the left and right hand sides of the eastern interface of the considered cell using the following MUSCL linear reconstruction formulae

$$\mathbf{q}_E^- = \mathbf{q}_{i,j}^{k+1/2} + \frac{\Delta x}{2}\nabla\hat{\mathbf{q}}_{i,j} \quad \text{and} \quad \mathbf{q}_E^+ = \mathbf{q}_{i+1,j}^{k+1/2} - \frac{\Delta x}{2}\nabla\hat{\mathbf{q}}_{i+1,j} \tag{7}$$

where $\nabla\hat{\mathbf{q}}_{i,j}$ and $\nabla\hat{\mathbf{q}}_{i+1,j}$ are evaluated by the flow variables at time level '*k*' and can directly adopt the values obtained during the predictor step, as suggested by other researchers [28]. The Riemann states are then used to solve the local Riemann problem to evaluate the numerical interface fluxes by implementing an HLLC approximate Riemann solver, as detailed in Liang and Borthwick [24]. After the interface fluxes across all four cell interfaces are properly calculated, the source terms are again discretised using finite differences. Finally, the flow variables are updated to the next time step according to equation (5).

2.3 Pressure model

The interaction between the flood waves and structures following a tsunami, storm surge or other extreme hydrodynamic events is physically very complex and may involve a number of different processes and forces, e.g. hydrostatic and hydrodynamic forces, buoyancy, waterborne debris impacts, wave loadings, and effects of scour and erosion [29]. This work will focus on the dominating loadings caused by hydrostatic and hydrodynamic pressure, which will be calculated using the flow variables obtained through solving the SWEs.

In open channel flows, any section of fluid is subject to a force function with two components according the momentum principle, which may be classified as hydrostatic pressure force and hydrodynamic force. The hydrodynamic force is typically the momentum of the fluid at the section under consideration, i.e. ρQU, where ρ is the density of water, Q is the total discharge through the cross-section and U is the average velocity. Representing the pressure force as P, the total force function is therefore

$$F = P + \rho QU \tag{8}$$

The total average pressure $\overline{f}$ can be obtained by dividing the normal cross-sectional area from both sides of the

above equation. Assuming a rectangular cross-section, $\overline{f}$ may be written as

$$\overline{f} = \overline{p}_s + \overline{p}_d = \frac{1}{2}\rho g h + \rho U^2 \tag{9}$$

where $\overline{p}_s = \rho g h/2$ is the hydrostatic pressure and $\overline{p}_d = \rho U^2$ corresponds to the hydrodynamic component, with U being the depth-averaged velocity normal to the structure surface. Obviously, the total pressure f at an arbitrary point within the fluid flow is given by

$$f = p_s + p_d = \rho g z + \rho U^2 \tag{10}$$

where $p_s = \rho g z$ and p_d are respectively the hydrostatic and hydrodynamic components of the point pressure, z is the depth from water surface to the point of interest, $\overline{p}_d = p_d$ since U is a constant in the vertical direction. At the current work, equations (9) and (10) are implemented within the aforementioned finite volume shallow flow model to estimate different pressure components.

3. Laboratory experiments

In order to better understand the physics of extreme hydrodynamic flows impacting on structures and obtain measured data for validating numerical models, laboratory experiments were designed and carried out in a 1m wide flume at the hydraulic laboratory in Hohai University, China. The flume is 35.5m long and a section of it is used in the current experimental tests, as shown in Fig.1.

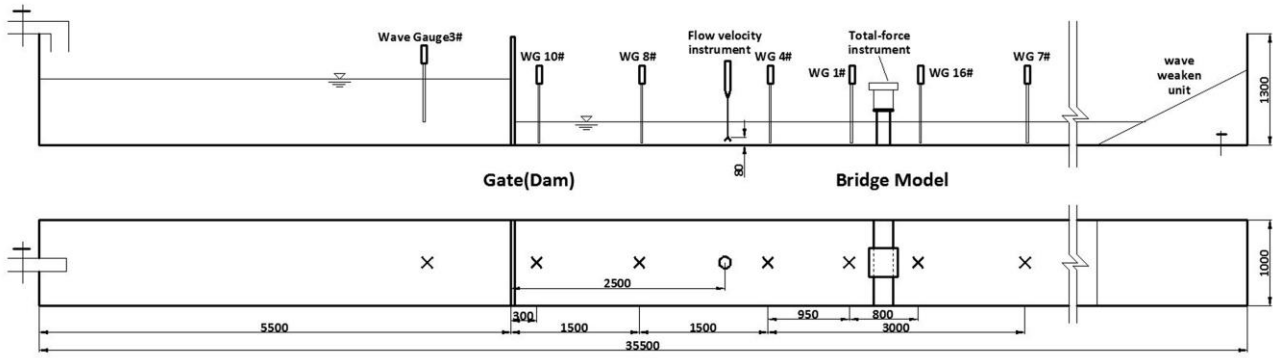

Fig.1 Vertical and horizontal views of the experimental flume and experimental setup (unit: mm)

Considering the fact that the overland flows caused by tsunamis or other severe coastal flood events typically move inland as a surge that is hydraulically similar to the rapidly propagating dam-break wave fronts. In case of flash flooding, the destructive 'walls of water' moving from upstream steep catchment to the downstream river channels and floodplain are also similar to dam-break waves. Therefore, dam-break waves were created to represent the extreme flow conditions under consideration during the current experiments. Dam-break waves have also been used by other researchers [3] to investigate the tsunami impacts.

The experimental layout is illustrated in Fig.1 with a gate installed in the channel to form an upstream reservoir. Two sidewalls of the channel is made of glasses supported and connected by steel brackets, while the material of the bottom is cement and the bottom was painted to be a smooth surface. During the experiments, the gate will be lifted instantaneously to produce dam-break waves. Scaled-down bridges with single and double piers are used to represent the impacted hydraulic structures. The dimensions of the bridges are presented in Fig.2. Over 30 experiments were performed with different water depth upstream and downstream of the dam, including dry bed cases, to investigate the impact of dam-break waves of different magnitudes on the structures. Time histories of water depth were recorded at seven calibrated wave gauges installed along the channel at locations as indicated in Fig.1. The sample interval of wave gauges is 0.003s. A high-resolution acoustic Doppler velocimeter (Nortek Vectrino Ⅱ) was used to measure water velocity. Six pressure sensors were fixed onto the bridge piers to measure the receiving impact and their locations are indicated in Fig.2. The acquisition frequency of pressure sensors is 5000Hz. All of the experimental measurements were analysed for better understanding the complex interacting processes between the sharp-fronted dam-break waves and structures and archived for model validation as presented in the next section.

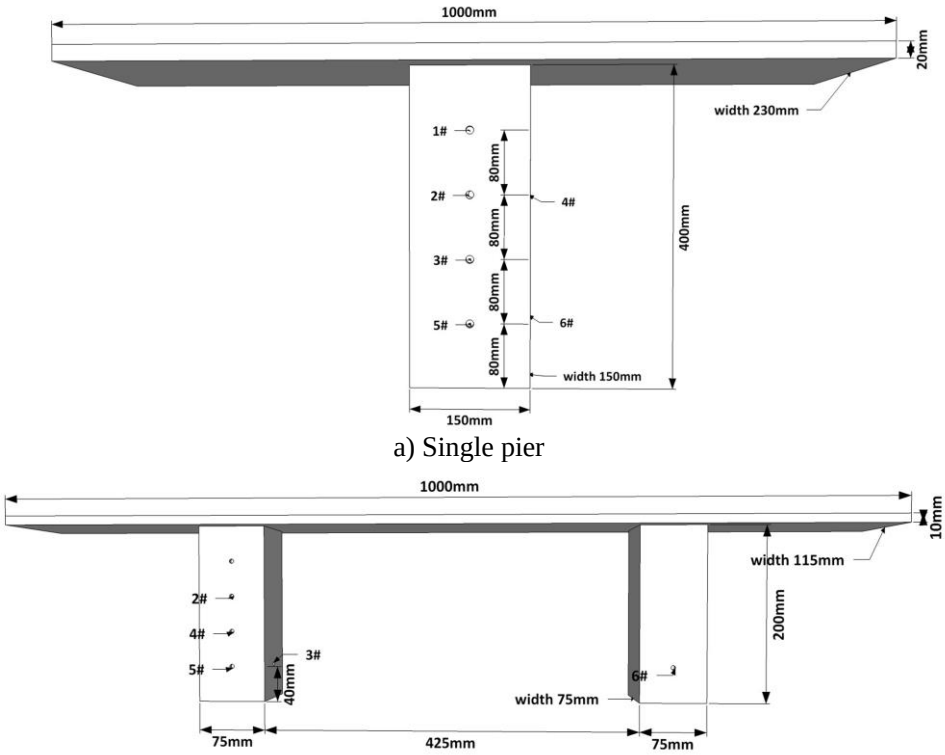

a) Single pier

b) Double piers

Fig.2 Bridge models and location of the pressure sensors

4. Numerical results

In this section, the current finite volume Godunov-type shallow flow model is validated for predicting the fluid-structure interaction and quantifying the impacting pressure under the extreme flow conditions induced by dam breaks by applying it to reproduce the laboratory experiments as introduced in Section 2. Among the series of experiments being conducted, two are selected herein to validate the numerical model, respectively for the bridge structure with a single pier or double piers. Open and closed boundary conditions are used during the numerical simulations and the detailed implementation can be found in Liang and Borthwick[24]. The CFL number in the Courant-Friedrichs-Lewy (CFL) criterion is set to 0.5 to ensure numerical stability. g = 9.81m/s^2 and ρ = 1000kg/m^3.

4.1 Single-pier test

The 15m × 1m flume section including the reservoir upstream of the dam and 9.5m long downstream valley that covers the bridge structure and all of the measuring devices is chosen to be the computational domain. The downstream boundary is 3.5m away from the last wave gauge. During the simulation, a uniform grid of 1500 × 100 cells is used to give a 0.01m spatial resolution in order to accurately represent the bridge structure and the locations of all of the measuring devices. The Manning coefficient is set to be 0.01s/m$^{1/3}$. Open boundary conditions are imposed at the downstream end of the computational domain and all other three domain edges are assumed to be closed. The simulation is run for 25s, with the initial still water depth of 0.4m and 0.198m upstream and downstream of the dam, respectively.

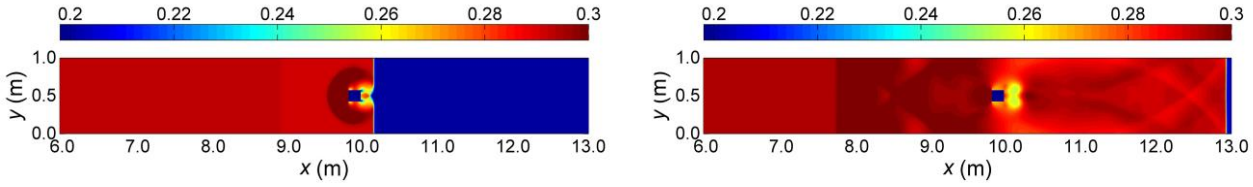

a)t = 2.5s b) t = 4s

Fig.3 Single pier: Water-structure interaction at sample output times

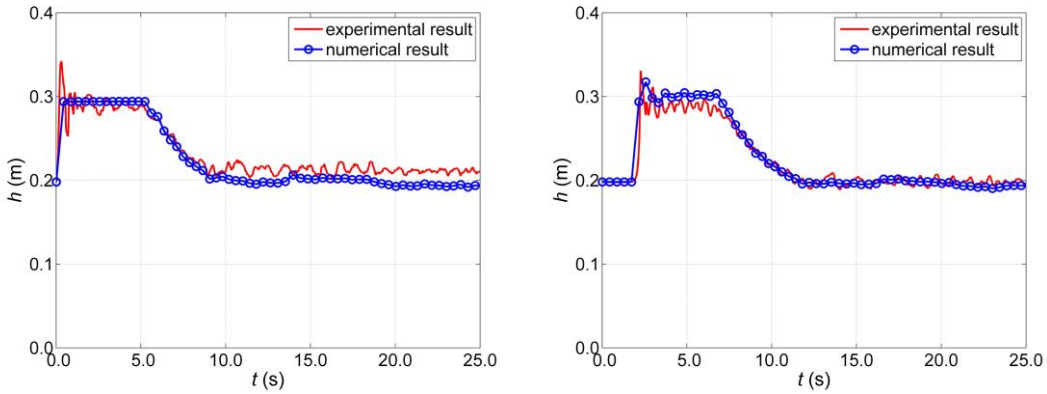

a) Wave gauge 10 b) Wave gauge 1

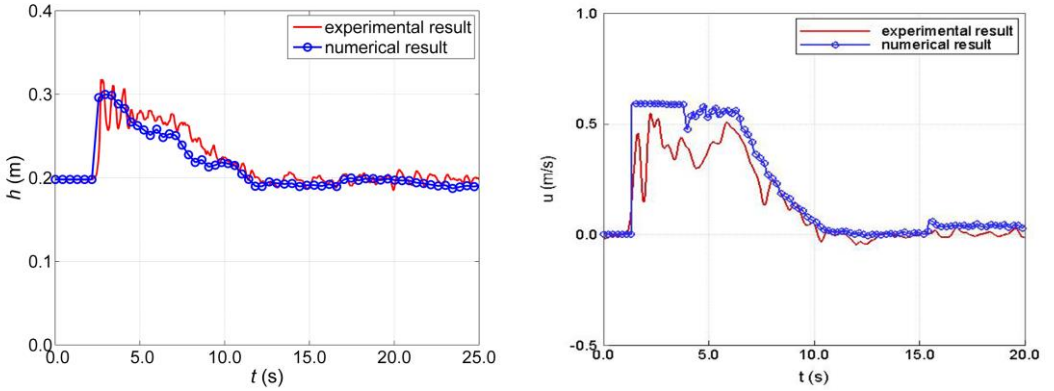

c) Wave gauge 16 d) Flow velocity

Fig.4 Single pier: Depth and velocity histories at sample gauges

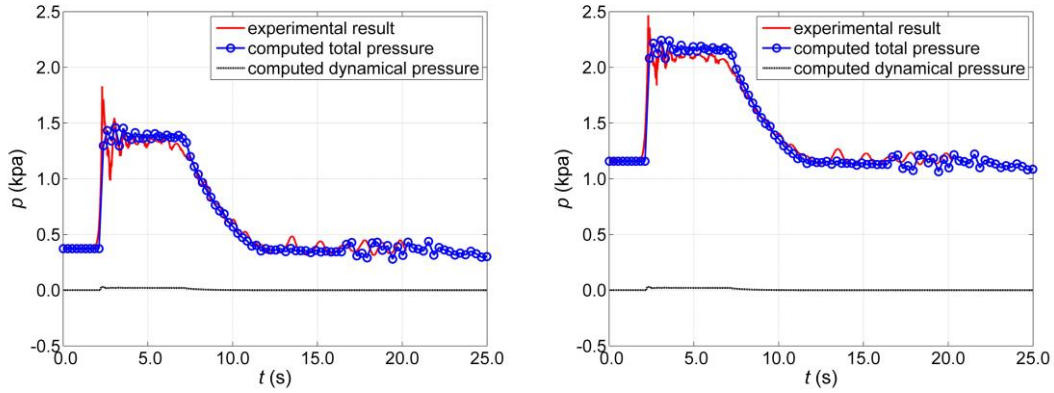

a) Sensor 3 b) Sensor 5

Fig.5 Single pier: Pressure histories at sample sensors

Fig.3 presents the simulation results in terms of plan-view water surface plots at two different output times. After the dam/gate opens at t = 0, a sharp-fronted shock wave immediately develops and propagates rapidly to downstream. At t = 2.5s, the shock wave has already attacked and passed the bridge structure. Upstream of the bridge, a semi-circular reflective shock is developed and travels towards the dam and the flume lateral walls; downstream of the bridge, the diffracted waves has met again at the mid-point of the channel and continues to move downstream as a straight front. At t = 4.0s, the wave-structure-boundary interaction has led to very complex wave patterns both upstream and downstream of the structure and the reflected shock front has evolved into a straight line propagating further upstream.

In order to verify the numerical prediction, the numerically predicted time histories of water depth are compared with those recorded at the seven wave gauges during the experiments. The numerical results are observed to agree satisfactorily with the measurements at all gauges, capturing accurately the magnitude and arriving time of the

shock. Fig.4 shows the numerical and measured depth and velocity histories at three sample gauges and the velocimeter. For pressure, we are more interested in the impact on the front side of the bridge pier facing the incoming shock. Fig.5 compares the numerically predicted time histories of pressure with those measured by the three pressure sensors that were located at the front side of the bridge and submerged before the experiment. The point pressure at all three gauges is observed to abruptly increase to a peak that lasts for a few seconds, following the impact of the dam-break shock. Apart from slightly over-predicting the peak at gauges, the numerical results agree reasonable well with the measurements.

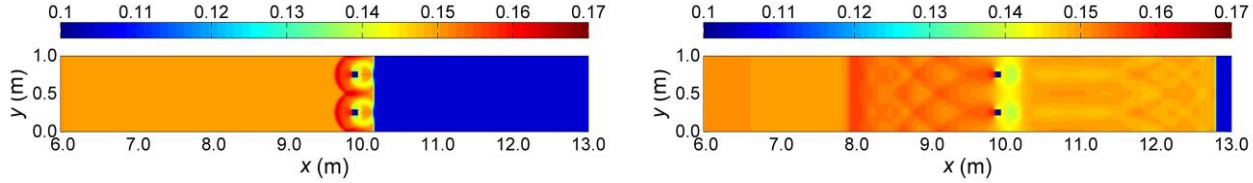

a) t = 3.5s b) t = 5.5s

Fig.6 Double piers: Water-structure interaction at sample output times

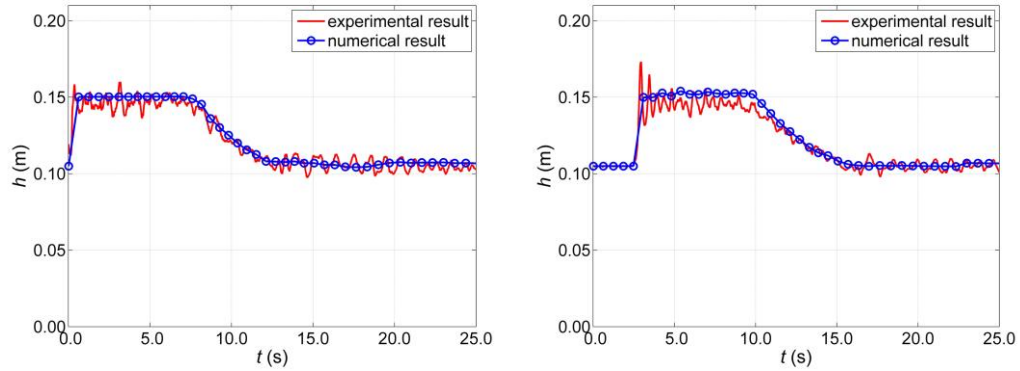

a) Wave gauge 10 b) Wave gauge 1

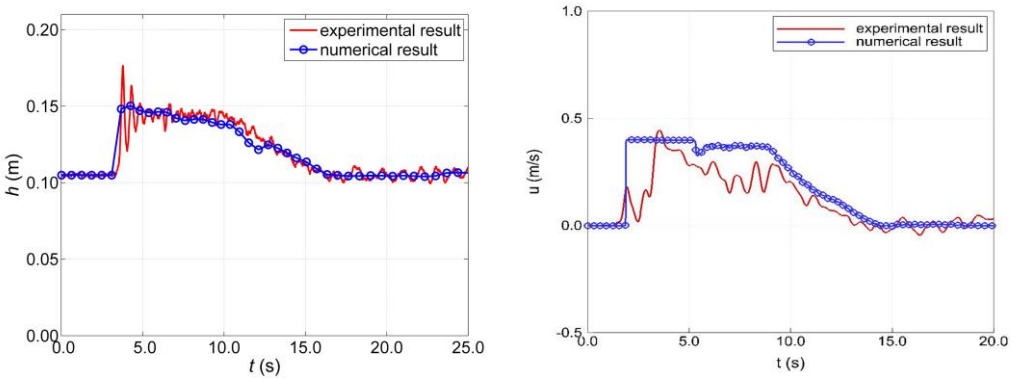

c) Wave gauge 16 d) Flow velocity

Fig.7 Double piers: Depth and velocity histories at sample gauges

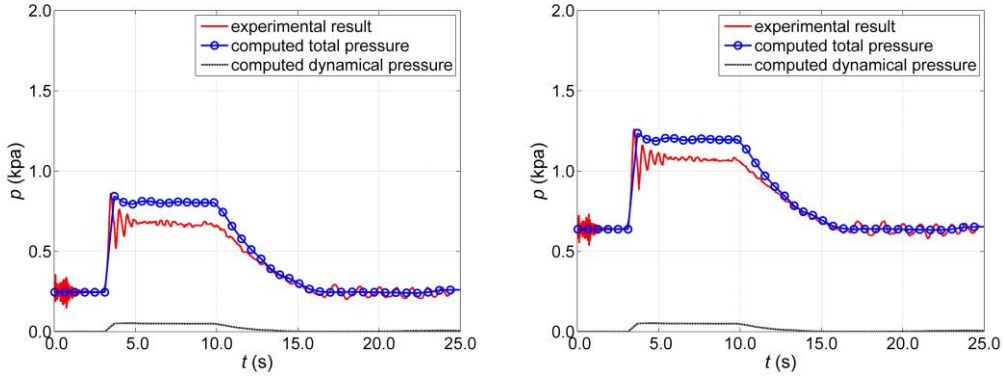

a) Sensor 4 b) Sensor 5

Fig.8 Double piers: Pressure histories at sample sensors

4.2 Double-pier test

In order to investigate the wave impacts on different types of structure, a model bridge with double piers was also used in the laboratory experiments. One of the double-pier experiments is selected to further demonstrate the performance of the current numerical model. In order to also consider different flow conditions during the fluid-structure interaction, the dam-break test with initial still water depth of 0.204m and 0.105m upstream and downstream of the dam is selected for this numerical simulation, while all other domain and numerical settings remain to be the same as the previous single-pier test.

Fig.6 depicts the plan-view water depth plots at two different output times. Similar to the single-pier test, the dam-break shock front developed following the dam failure at $t = 0$ travels rapidly to downstream. Due to the shallower initial water depth, the shock wave propagates at a slower speed compared to the single-pier case where the downstream initial depth is 0.198m. The sharp wave front hits the two bridge piers slightly before $t = 3.5$s, which immediately results in the formation of two semi-circular reflected shocks propagating upstream towards the reservoir. At $t = 5.5$s, very complex wave patterns have been developed following the wave-structure-boundary interaction, as also observed at the single-pier test.

The comparison between the numerically predicted and experimentally measured time histories of water depth at the three sample gauges is presented in Fig.7 and close agreement is again achieved. For pressure, only two of the pressure sensors at the front side the bridge pier were initially submerged to give accredited data. Comparison is therefore made between the numerical and experimental data at these two sensors and presented in Fig.8. Similar to the single-pier test, the numerical solutions compare satisfactorily with the measurements except for slight over-prediction at the peak. From the results, it is also interesting to notice that the wave-structure interaction, as indicated by the time histories of water depth and pressure, presents similar processes for both of the cases being simulated, i.e. the two-pier structures seem to receive similar wave impact as those single-pier structures. However, this conclusion may be dependent on the magnitude of the incoming shock.

5. Conclusions

In this work, physical experiments have been conducted to better understand the physical processes following the impact of extreme hydrodynamic flow on structures, which may occur following a flood event caused by dam breaks, flash floods, tsunamis or storm surges. Due to the hydraulic similarity between these flood flows and dam-break waves, dam-break experiments were designed and carried out in the hydraulic laboratory at Hohai University, China to investigate the extreme flow impact on two types of bridge structures. As observed at the sample results being shown in Section 4, the impact of dam-break shock wave on both types of structures indicated by pressure variation presents a sharp rise following the arrival of the incoming dam-break wave front. The pressure is much larger than that measured at the normal flow conditions and must be properly taken into account during structural design.

In order to facilitate wider and more flexible applications in hazard management, city planning and structural design, a finite volume Godunov-type model solving the two-dimensional SWEs has been validated through application to reproduce two selected laboratory experiments. The current model is able to predict water depth and pressure that closely agree with the laboratory measurements. Particularly, the model resolves accurately the shock-like flow discontinuities following the dam breaks and reliably predicts the arriving time of the wave front. The model has also been further developed to enable pressure calculation in order to quantify the flood impact on structures and the new model component has also been successfully validated during the numerical simulations. Therefore, the model may potentially provide a robust tool for a wide range of field-scale applications and can be also used for calibrating simplified models or formulae for structural design.

Acknowledgments

This work is supported by the following projects: National Natural Science Foundation of China (NSFC) standard research award (Ref. 51379074), the Chinese Government 'Recruitment Program of Global Experts' and the Royal Society and NSFC cost share International Exchanges award (Royal Society Ref. IE131297; NSFC Ref. 51411130125).

References

[1] DALRYMPLE R. A., KRIEBEL D. L. Lessons in engineering from the tsunami in Thailand[J]. **The Bridge, National Academy of Engineering**, 2005, 35(2): 4-13.

[2] ROSSETTO T., PEIRIS N. and POMONIS A. et al. The Indian Ocean tsunami of December 26, 2004: observations in Sri Lanka and Thailand[J]. **Natural Hazards**, 2007, 42(1): 105-124.
[3] NISTOR I., PALERMO D. and CORNETT A. et al. Experimental and numerical modeling of tsunami loading on structures[C]. **33rd International Conference on Coastal Engineering**. Santander, Spain, 2012.
[4] STOCKER T., QIN D. and PLATTNER G. et al. IPCC, 2013: climate change 2013: the physical science basis[R]. **Contribution of working group I to the fifth assessment report of the intergovernmental panel on climate change**. 2013.
[5] KENDON E. J., ROBERTS N. M. and FOWLER H. J. et al. Heavier summer downpours with climate change revealed by weather forecast resolution model[J]. **Nature Climate Change**, 2014.
[6] The Royal Society. Resilience to extreme weather, The Royal Society Science Policy Centre report, DES3400, 2014.
[7] KELMAN I., SPENCE R. An overview of flood actions on buildings[J]. **Engineering Geology**, 2004, 73(3): 297-309.
[8] JONKMAN S. Loss of life caused by floods: an overview of mortality statistics for worldwide floods[R]. 2003, Delft Cluster.
[9] ROOS W. Damage to buildings. 2003, Delft Cluster.
[10] PISTRIKA A. K., JONKMAN S. N. Damage to residential buildings due to flooding of New Orleans after hurricane Katrina[J]. **Natural Hazards,** 2010, 54(2): 413-434.
[11] ROBERTSON I. N., RIGGS H. R. and YIM S. C. et al. Lessons from Hurricane Katrina storm surge on bridges and buildings[J]. **Journal of Waterway, Port, Coastal, and Ocean Engineering**, 2007, 133(6): 463-483.
[12] WU J., ZHANG H., and Rui Y., et al. Numerical modeling of dam-break flood through intricate city layouts including underground spaces using GPU-based SPH method[J]. **Journal of Hydrodynamics**, Ser. B, 2013, 25(6): 818-828.
[13] FRANZ S., TOBIAS B. and HOU J., et al. A model for overland flow and associated processes within the Hydroinformatics Modelling System[J]. **Journal of Hydroinformatics**, 2014, 16(2): 375–391.
[14] LIANG Q., SMITH L. S. A high-performance integrated hydrodynamic modelling system for urban flood simulations. **Journal of Hydroinformatics**, 2015, 17(4): 518–533.
[15] HUNTER N., BATES P. and NEELZ S. et al. Benchmarking 2D hydraulic models for urban flood simulations[J]. **Proceedings of the Institution of Civil Engineers: Water Management**, 2008, 161(1): 13-30.
[16] LIANG Q., DU G. and HALL J. W. et al. Flood inundation modeling with an adaptive quadtree grid shallow water equation solver[J]. **Journal of Hydraulic Engineering**, 2008, 134(11): 1603-1610.
[17] VACONDIO R., ROGERS B. and STANSBY P. et al. SPH modeling of shallow flow with open boundaries for practical flood simulation[J]. **Journal of Hydraulic Engineering**, 2012, 138(6): 530-541.
[18] GUINOT V. Multiple porosity shallow water models for macroscopic modelling of urban floods[J]. **Advances in Water Resources**, 2012, 37: 40-72.
[19] SOARES-FRAZO S., LHOMME J. and GUINOT V. et al. Two-dimensional shallow-water model with porosity for urban flood modelling[J]. **Journal of Hydraulic Research**, 2008, 46(1): 45-64.
[20] SCHUBERT J. E., SANDERS B. F. Building treatments for urban flood inundation models and implications for predictive skill and modeling efficiency[J]. **Advances in Water Resources**, 2012, 41: 49-64.
[21] GALLEGOS H. A., SCHUBERT J. E. and SANDERS B. F. Two-dimensional, high-resolution modeling of urban dam-break flooding: a case study of Baldwin Hills, California[J]. **Advances in Water Resources**, 2009, 32(8): 1323-1335.
[22] GHADIMI P., REISINEZHAD A. Numerical simulation of flood waves and calculation of exerted forces on the cylindrical piers in contraction channels with different cross section profiles[J]. **Journal of Hydroinformatics**, 2012, 14(2): 366-385.
[23] LIANG Q. A coupled morphodynamic model for applications involving wetting and drying[J]. **Journal of Hydrodynamics**, Ser. B, 2011, 23(3): 273-281.
[24] LIANG Q., BORTHWICK A. G. Adaptive quadtree simulation of shallow flows with wet–dry fronts over complex topography[J]. **Computers & Fluids**, 2009, 38(2): 221-234.
[25] GREENBERG J. M., LEROUX A. Y. A well-balanced scheme for the numerical processing of source terms in hyperbolic equations[J]. **SIAM Journal on Numerical Analysis**, 1996, 33(1): 1-16.
[26] TORO E. F., SPRUCE M. and SPEARES W. Restoration of the contact surface in the HLL-Riemann solver. **Shock waves**, 1994, 4(1): 25-34.

[27] VAN LEER B. Towards the ultimate conservative difference scheme. V. A second-order sequel to Godunov's method[J]. **Journal of Computational Physics**, 1979, 32(1): 101-136.
[28] HU K., MINGHAM C. G. and CAUSON D. M. Numerical simulation of wave overtopping of coastal structures using the non-linear shallow water equations[J]. **Coastal Engineering**, 2000, 41(4): 433-465.
[29] YIM S. C. Modeling and simulation of tsunami and storm surge hydrodynamic loads on coastal bridge structures[C]. **Proceedings of the 21st US-Japan Bridge Engineering Workshop**, 2005.